ADVANCED MATERIALS INTERFACES
Open Access
www.advmatinterfaces.de

Amplified Sensitivity in SERS Detection of L1CAM With Silver Plasmonic Mesoporous Silica Capsules on an Imprinted Films

Yuselis Castaño-Guerrero, Belén Arjones-Fernández, Felismina T.C. Moreira, Ramon A. Alvarez-Puebla, Miguel A. Correa-Duarte, H. Águas, and M. Goreti F. Sales**

This study presents a novel approach for dual detection, leveraging a combination of a Raman reporter-bearing nanomaterial and molecular imprinting polymers (MIP). A core-shell Au-Ag nanoparticles (Au-Ag NPs) encapsulated in mesoporous silica nanocapsules (Au-Ag NCs) and a new MIP-based material targeting L1CAM are used. The MIP prepared via surface imprinting on a carbon screen-printed electrode (C-SPE) used thionine (TH) as a monomer. The plasmonic Au-AgNCs are further functionalized with the Raman reporter 4-mercaptobenzoic acid (MBA) and anti-L1CAM for selective detection by surface-enhanced Raman scattering (SERS) spectroscopy. The biosensor's analytical performance is evaluated using both SERS and electrochemical impedance spectroscopy (EIS). EIS analysis reveals a linear response within the concentration range of 0.1 to 100 ng mL^{-1} in buffer and serum samples. SERS demonstrates a sensitivity ten times higher than EIS. Selectivity study demonstrates the biosensor's excellent specificity toward L1CAM, with minimal interference from other compounds such as creatinine, glucose, and carbohydrate antigen 19-9 (CA 19-9). The Raman signal from the reporter molecule correlates with increasing L1CAM concentrations, reinforcing the analytical findings obtained through electrochemical analysis. Thus, the combination of dual detection and recognition capabilities presents promising potential for detecting diverse biomarkers, especially in critical scenarios where reducing false-positive or false-negative errors is crucial.

1. Introduction

Many chemical modifications of metallic nanoparticles (NPs) aim to improve their chemical/mechanical stability and fine-tune the surface properties in terms of electrical charge or chemical functionalities.[1] This can include layered core structures,[2–4] which prevent agglomeration or deformation of the metallic NPs. Mesoporous silica coatings of metallic NPs have gained attention in this context, due to their numerous advantages, such as high surface area, controllable pore size, high thermal stability, and easy surface functionalization.[5]

NPs with a metallic core and a suitably designed protective shell are of interest for surface-enhanced Raman spectroscopy (SERS), which aims to maximize the signal enhancement of specific Raman reporter molecules.[6] Gold NPs (AuNPs) have been used in SERS in many forms and with many coatings, including silica, with different thicknesses, sizes, and shapes of the plasmonic core, confirming high enhancement factors.[7,8] Despite the many studies on AuNPs, silver NPs (AgNPs) have also been used[9,10] and out perform AuNPs due to their special optical properties[4]; AgNPs have a much sharper and stronger plasmon resonance compared to AuNPs.

The use of AgNPs in SERS is hindered by the low chemical stability of Ag,[11,12] for which core-shell Ag nanostructures have been developed.[9,10,13,14] A shell with a bimetallic core of Au/Ag can further combine the advantages of both metals in

Y. Castaño-Guerrero, F. T. Moreira, M. G. F. Sales
BioMark@ISEP/CEB-LABBELS
School of Engineering of the Polytechnic Institute of Porto
Rua Dr. António Bernardino de Almeida, 431, Porto 4249-015, Porto, Portugal
E-mail: goreti.sales@eq.uc.pt

The ORCID identification number(s) for the author(s) of this article can be found under https://doi.org/10.1002/admi.202400299

DOI: 10.1002/admi.202400299

Y. Castaño-Guerrero, F. T. Moreira, M. G. F. Sales
BioMark@UC/CEB-LABBELS
Department of Chemical Engineering
Faculty of Sciences and Technology
University of Coimbra
R. Silvio Lima, Coimbra 3030-790, Coimbra, Portugal

B. Arjones-Fernández, M. A. Correa-Duarte
CINBIO
Universidade de Vigo
Vigo 36310, España, Spain
E-mail: macorrea@uvigo.es

B. Arjones-Fernández, M. A. Correa-Duarte
Biomedical Research Networking Center for Mental Health (CIBERSAM)
Southern Galicia Institute of Health Research (IISGS)
Vigo 36310, España, Spain

terms of SERS signal output. In particular, the combination of Au and Ag provides easy morphology control and strong plasmonic properties, leading to higher SERS intensity than the pure NPs alone.[15]

When these metal NPs are used for SERS sensing, a biological recognition element is desired to improve the accuracy of the determination. Molecularly imprinted polymers (MIP) have been shown to be successful biological recognition elements in this context.[16] MIP are prepared by forming a complex between the target molecule and selected functional monomers that undergoes appropriate polymerization. When the target molecule is removed, the vacancies formed on the polymeric network can selectively capture the imprinted target molecules.[17,18]

Since the first report on MIP-SERS sensors in 2003 by Kostrewa et al.,[19] special attention has continued to be paid to this area. According to the recent review by Guo et al, particle-based MIP-SERS sensors are divided into three categories.[18] First, there are the MIP-over-SERS sensors (M-o-S),[20–22] which are characterized by presenting SERS nanoparticles coated by MIP surface imprinting. Secondly, there are SERS on MIP (S-o-M),[23] in which a well-tuned number of NPs create a "hot spot" in the sensor structure. And finally, the MIP mixed with SERS (M-m-S),[24] which are easier to fabricate compared to the previous ones and avoid complex SERS substrates.

This study presents an innovative chip-based MIP-SERS sensor, fabricated employing a particle-based sensor approach, boasting a significantly larger surface area compared to conventional particle-based sensors.[17,18,25] This advancement is achieved through the utilization of a novel plasmonic mesoporous-silica@Ag nanocapsules (AgNCs). Our research delivers enhanced amplification of the SERS signal, surpassing the capabilities of conventional AuNPs or AgNPs. Specifically, we employed Au-AgNPs encapsulated in mesoporous silica capsules and 4-mercaptobenzoic acid (MBA) as Raman tags, which are absorbed onto the Ag surface to serve as the SERS substrate. We showcase this improvement through the direct detection of the L1 cell adhesion molecule (L1CAM) within a MIP sensor platform constructed electrochemically on screen-printed carbon electrodes (C-SPE). Furthermore, we introduce a sandwich detection approach by binding L1CAM antibodies to the SERS substrate, combining MIP and antibody methodologies for enhanced sensitivity and selectivity. The optimization of our system involved meticulous consideration of various parameters, guided by comprehensive analysis of EIS and SERS data.

R. A. Alvarez-Puebla
ICREA—Institució Catalana de Recerca i Estudis Avançats
Barcelona 08010, Spain
R. A. Alvarez-Puebla
Department of Physical and Inorganic Chemistry
Universitat Rovira i Virgili
Tarragona 43007, Spain
H. Águas
CENIMAT
i3N
Departament of Material Sciences
Faculty of Sciences and Technology
New University of Lisbon, and CEMOP/UNINOVA
Campus da Caparica, Caparica 2829 - 516, Lisboa, Portugal

2. Experimental Section

2.1. Equipment

The potentiostat/galvanostat from Metrohm Autolab was used for electrochemical measurements. It was equipped with an impedimetric module and was controlled by the NOVA 2.0 software. Commercially available C-SPE were used (DropSens, DRP-C110), which combine working and counter electrodes made of carbon as well as reference electrodes and electrical contacts made of silver. Raman spectra were recorded using a Renishaw Invia system with a high resolution grating of 1200 g cm^{-1} and an acquisition time of 10 s or a Thermo DXR Raman confocal microscope. The laser (785 nm) was focused on the samples through a 50× objective with a power of 2.47 mW. Transmission electron microscopy (TEM) was performed using a JEOL JEM 1010 transmission electron microscope operating at an accelerating voltage of 100 kV.

2.2. Reagents and Solutions

All chemicals were of analytical grade and the water was ultra-pure Milli-Q. Potassium hexacyanoferrate III ($K_3[Fe(CN)_6]$), potassium hexacyanoferrate II ($K_4[Fe(CN)_6]$) trihydrate, sodium phosphate dibasic dihydrate (Na_2HPO_4), and *ortho*-phosphoric acid 85% (H_3PO_4) were purchased from Riedel-de-Häen; sodium chloride (NaCl), ascorbic acid, 4-mercaptobenzoic acid (MBA), polyvinylpyrrolidone, poly(diallyldimethylammonium chloride) solution 20 wt.% in H_2O (MW: 400000–500000), L1CAM antigen (4.7 mg mL^{-1}, 34 kDa) and anti-L1CAM (IgG, polyclonal, produced in rabbit) were purchased from Sigma-Aldrich; silver nitrate ($AgNO_3$) from Fluka; sodium phosphate dibasic dihydrate, 99.5% ($Na_2HPO_4.2H_2O$) from Panreac; sodium dihydrogen phosphate dihydrate ($NaH_2PO_4.2H_2O$) from Scharlau; foetal bovine serum from Alfa Aesar. Sulfuric acid (H_2SO_4) was purchased from BDH; thionin acetate from Acros Organics.

2.3. Synthesis of the Au-Ag/SiO_2 m-Capsules

A more detailed description of the synthesis and characterization of the AgNCs has been presented by González-Domínguez et al., 2017.[26] As a first step, the functionalization of polystyrene (PS) beads (Ikerlat Polymers, 500 nm) was achieved by employing poly(allylamine hydrochloride) (PAH, Mw = 17500).[27] In this process, PAH was dissolved in 0.5 M NaCl (pH 5.0) with a polymer concentration of 1 mg mL^{-1}. Subsequently, a positively charged PAH solution (25 mL) was added to the PS beads (12.5 mg) and stirred at room temperature for 30 min. To remove excess reagents, four cycles of centrifugation and redispersion were performed using water (9000 rpm, 40 min each). This procedure endowed the PS particles with the requisite electrostatic charge for the subsequent adsorption of Au nanoparticles.

The synthesis and adsorption of AuNPs (3 nm, [Au] = 1.0 × 10^{-4} M) were carried out following established protocols by Duff et al., 1993.[28] Au seeds (1–3 nm; [Au] = 1 × 10^{-3} M) were synthesized add 9.1 mL of water to a beaker and shake it. Then, was added 0.3 mL of NaOH (0.2 M) solution. In this solution under

stir was added 0.2 mL of THCP, followed by 0.4 mL of HAuCL4 (25 mM) solution. At this point the stirred solution changes to a dark brown color. Continue stirring for ≈15 min. The resulting solution was stored at 4 °C until used.

The AuNPs solution (5.0 mL) was added under sonication to the PS beads solution (50 mL, 0.25 mg mL^{-1}) and stirred at room temperature for 30 min. The resulting suspension was then subjected to centrifugation to remove excess AuNPs via three cycles of centrifugation and redispersion with water (3500 rpm, 40 min each). The sediment was redispersed in water (12.5 mL) to achieve a final concentration of 1.00 mg mL^{-1}, with reference to the PS template.

Silica coating was carried out following established procedures.[29] In brief, the previous PS@Au suspension (12.5 mL) was added dropwise under sonication to a solution containing cetyltrimethylammonium bromide (CTAB, 312.5 mg), Milli-Q water (125 mL), ethanol (50 mL), and an aqueous ammonia solution (28 wt%, 1.5 mL). After sonication for 15 min, a tetraethyl orthosilicate ethanolic solution (5% v/v, 2.06 mL) was added dropwise under continued sonication. The mixture was then stirred for 17 h to achieve homogeneous silica growth. The resulting PS@Au@SiO_2 particles were subjected to four cycles of centrifugation and redispersion in ethanol (3,500 rpm, 20 min each). Finally, the organic templates (PS and CTAB) were eliminated by calcination at 600 °C for 4 h, yielding the void@Au@mSiO_2 composite.

In the second step of growing for Au/Ag (onto the previous void@Au@mSiO_2) was obtained the AgNC/AuNC. The growth of Au-Ag nanoparticles inside the hollow cavity was achieved using Au NPs as seeds. Silver nitrate (10 mM, 1 mL) was added to 0.5 mL of the Au/mSiO_2 nanocapsules suspension (1.25 mg mL^{-1}) with vigorous stirring. After 5 min, 10 µL of ascorbic acid (10 mM) was added to the solution, resulting in a color change from red to brown due to the reduction of Ag^+. The sample was stirred for an additional 5 min before undergoing centrifugation and washing with ethanol (3500 rpm, 10 min) to remove excess reagents and obtain the AgNCs. Subsequently, the Raman reporter solution (MBA, 1.0 × 10–4 M) was combined with the AgNCs and mixed for 1 h in the dark. The solution was then washed with ethanol and water (3500 rpm, 10 min) to eliminate unbound MBA. For PVP functionalization, 25 mg PVP-30k was dissolved in 0.75 mL water. 375 µL of this polymer solution was added to the AgNCs (625 mg) and stirred for 18 h at room temperature. Subsequently, the PVP excess was removed by three centrifugations and redispersing cycles with water (3500 rpm, 10 min). Finally, the product was dispersed again in water (0.5 mL). For obtain AuNC was followed the same procedure used before with AgNC, but instead, Ag was used Au^{3+} to reduce to Au^+.[29]

The obtained structures Au-Ag(MBA)/mSiO_2/PVP were functionalized with poly(diallyldimethylammonium chloride) solution 20 wt.% in H_2O (PDDA, MW: 400000–500000). For this purpose, PDDA was dissolved in a 0.5 M NaCl solution (pH 5.0) with a final polymer concentration of 2 mg mL^{-1}. Then 1.5 mL of the positively charged solution was added to the capsules (625 mg) and stirred for 30 min at room temperature. The excess of reagents was removed by three cycles of centrifugation-redispersion (3500 rpm, 10 min) the first two with water and the last with phosphate buffer (PhB), as this was the appropriate medium for the addition of the antibody for L1CAM (Ab). This polyelectrolyte film provided the necessary electrostatic charge surface to facilitate the subsequent adsorption of the antibody.

The AgNCs were redispersed in 200 µL PhB and 100 µL Ab (0.03 mg mL^{-1}) was added. The whole was stirred for 1 h, followed by three cycles of centrifugation and redispersion with PhB. Finally, the resulting material was redispersed in 200 µL buffer (3.125 mg mL^{-1}).

2.4. SERS and Electrochemical Measurements

For the SERS measurements, a volume of 5 µL of the solution containing the dispersed Ag/MBA/mSiO_2/PVP/PDDA/Ab material (3.125 mg mL^{-1}) was used, which was poured overnight onto the biosensor with different concentrations of L1CAM. Then the surface was washed, and the biosensor was prepared for Raman calibration with different concentrations of L1CAM as described below for the electrochemical calibration curves.

The electrochemical measurements were used to follow the construction of the biosensor and its calibration. For this purpose, CV and EIS were used in the presence of a standard redox probe, $[Fe(CN)_6]^{3-/4-}$ covering the 3-electrode system. EIS shows the electron transfer and diffusion processes at the electrode/electrolyte interface in the form of a Nyquist plot. CV shows the current changes as a function of a series of applied potentials. In the EIS tests, a frequency range of 0.1 to 1 × 105 Hz was used, with an amplitude of 0.01 V and a number of 50 frequencies.

2.5. Preparation of MIP

The MIP synthesis was supported electrochemically and carried out on the C-SPE surface. A schematic representation can be found in **Figure 1**. In general, the preparation of MIP involved several steps: i) purification, ii) preparation of the electrode to receive the protein, iii) protein binding, iv) electropolymerization of the monomer, and v) removal of the protein template. Each of these phases was monitored by electrochemical impedance spectroscopy (EIS).

In the cleaning phase, a H_2SO_4 solution (0.5 M) was used, and the electrodes were subjected to 15 cycles of cyclic voltammetry (CV) between −0.2 and +1.2 V at a scan rate of 0.05 V s^{-1}. Then the working electrode was covered with TH (10^{-3} M) for 1 h at room temperature.

Subsequently, the C-SPE modified with TH (C-SPE/TH) was incubated with L1CAM (0.01 mg mL^{-1}) for 1 h. Electropolymerization was performed with TH solution dripped onto the 3-electrodes. A CV between −0.4 and +0.4 V was used at a scan rate of 0.050 V s^{-1} for 15 cycles. Subsequently, the polymer-modified electrode was incubated with oxalic acid (0.5 M) for 2 h to remove the L1CAM template, as described in a previous study.[30] A control sample, a non-imprinted polymer (NIP), was prepared using the same procedure without L1CAM.

2.6. Electrochemical Measurements

The electrochemical measurements to calibrate the biosensor were performed in a 5 mM $[Fe(CN)_6]^{3-/4-}$ solution prepared in

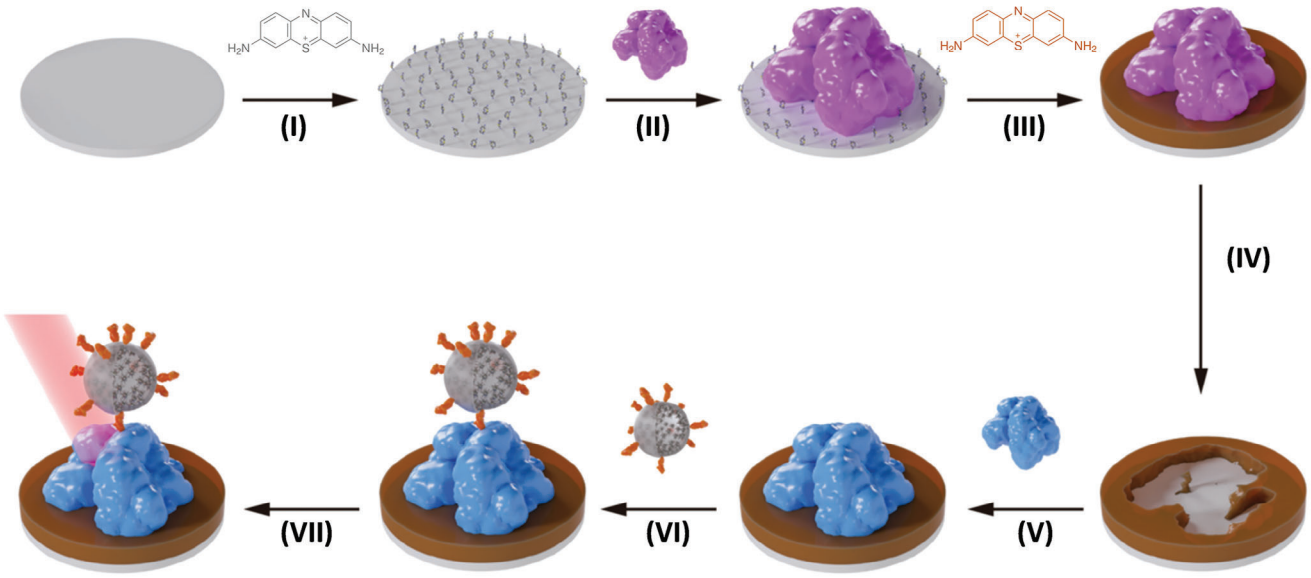

Figure 1. Schematic representation of the biosensor setup followed by incubation of L1CAM and the molecular probe for SERS readings. I) casting of TH on the clean C-SPE; II) casting of L1CAM; III) electropolymerization of TH; IV) removal of L1CAM; V) binding with L1CAM (from samples or standards); VI) binding of AgNCs with Ab; VII) and SERS measurement in a confocal Raman spectroscope.

PhB 0.1 M with a pH of 7.4 (0.0754 M Na_2HPO_4 and 0.0246 M NaH_2PO_4). The L1CAM standard solutions used in the calibrations ranged from 0.1 to 100 ng mL^{-1} and were prepared by diluting the commercial protein in PhB buffer or in FBS diluted in PhB (1:100). Each solution was allowed to stand on the electrode for 20 min at room temperature. The selectivity study was performed in a similar manner with interfering species. The interfering solutions, also prepared in PhB, were 7.0×10^{-4} g mL^{-1} glucose, 1.0×10^{-3} g mL^{-1} creatinine, and 37 U mL^{-1} CA 19-9.

3. Results and Discussion

3.1. Au-Ag/mSiO$_2$ Nanocapsules Raman Probes

The novel plasmonic Raman probe (depicted in **Figure 2a**) was synthesized by initially depositing 3 nm gold seeds onto positively-charged polystyrene (PS) particles with a diameter of 500 nm, employing electrostatic layer-by-layer (LbL) self-assembly. Subsequently, the resulting PS@Au particles underwent a coating process with a uniform mesoporous silica layer measuring 30 nm in thickness, accomplished by employing tetraethoxysilane in ethanol. The polymeric core was then eliminated through calcination at 600 °C for 4 h. Representative transmission electron microscopy (TEM) images, as depicted in Figure 2b illustrate the capsules' morphology before and after calcination, clearly revealing the silica shell and individual Au seeds within their inner cavity. Further, the gold seeds underwent selective overgrowth inside the hollow cavity of the capsule through a catalyzed epitaxial reduction of Ag ions with ascorbic acid, as illustrated in Figure 2c, resulting in a particle size of ≈15–20 nm to maximize their optical enhancement performance. Additionally, X-ray energy dispersive spectroscopy (XEDS) analyses (as shown in Figure 2b,c) provide compelling evidence of exclusive growth of AgNPs within the silica capsule's inner space, with no traces of gold detected on the outer surface.

In Figure 2b shows the evolution of the localized surface plasmon resonance (LSPR) from the initial gold nanoparticle to their growth with Ag. Initially, just appear in the UV-vis spectra a signal at 520 nm characteristic of isolated AuNPs. Remarkably, following silver overgrowth, the LSPR profile gradually broadens and shifts toward shorter wavelengths, indicating the growth of Ag as well as an extensive plasmonic coupling and the creation of electromagnetic hot spots. The subsequent addition of MBA molecules facilitated their binding to Ag through thiol groups once they diffused into the inner cavity of the plasmonic capsules via the silica mesopores. This process led to the generation of an intense SERS signal of MBA as a molecular probe.

The resulting SERS spectra confirmed that MBA was adsorbed/attached to the Ag surface (**Figure 3B**). The characteristic spectrum of MBA showed two Raman bands at 1078 and 1585 cm^{-1}, which were associated with the characteristic vibrations of the C-H bond of the aromatic ring and the C = C vibrations, respectively.[15,31] The bands at 845 and 1420 cm−^{1} belong to δ(COO−) and ν(COO^-), respectively. The band observed at 719 cm^{-1} was assigned to the vibration γ(CCC) outside the aromatic ring (shown the table in Figure 3A).[32]

Overall, the intensity of the spectra was high when compared to the typical Raman signal of the MBA alone. This confirmed the attainment of a strong electromagnetic field around the silver, referred to as a "hot spot".[18] This effect was further enhanced because each AgNCs acted as a second amplifier of the "hot spots", as a single capsule contained multiple hot spots of MBA molecules next to the Ag, most of which should produce a Raman signal. Since a single capsule may be signaling a single L1CAM protein, the Raman signal generated by a single protein is immensely amplified with our approach. In addition, the shell around the silver is expected to have a protective effect against

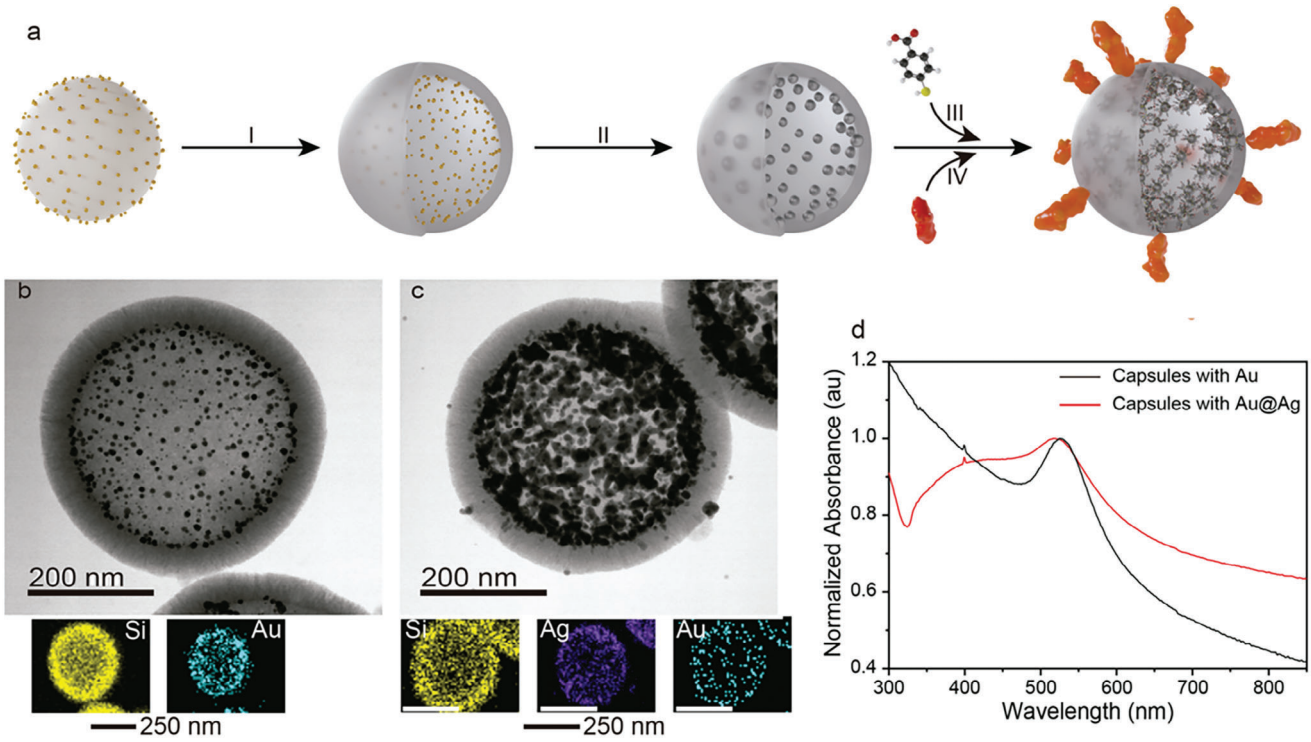

Figure 2. a) Schematic representation of the synthetic approach to obtain the Raman probe on the AgNCs, the transmission electron microscopy images of b) Si-Au (seed) and c) Si/Au-Ag nanocapsules; and d) the UV–vis spectra of aqueous dispersions of Si-Au and Si-Ag nanocapsules. I) coating with a mesoporous silica layer the gold seeds/polystyrene particles; III) calcination to eliminate the polymeric core; III) addition of 4-mercaptobenzoic acid to the system; addition of antibodies against the L1CAM.

A) Peak Frenquency (cm^{-1})	assignment
719	γ(CCC)
845	$\delta(COO^-)$
1078	$\nu(CC)_{ring}$
1420	$\nu(COO^-)$
1585	$\nu(CC)_{ring}$

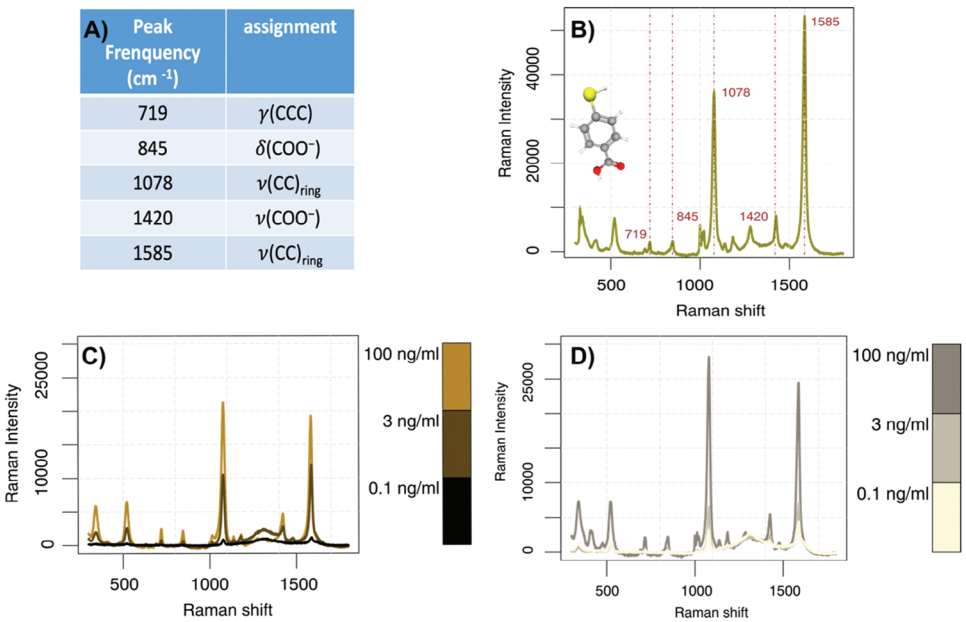

Figure 3. A) Table of characteristics Raman peaks for MBA, and B) the typical Raman spectra obtained for MBA. C,D) SERS spectra obtained with AuNCs and AgNCs incubated in the biosensor at different concentrations (0.1, 3, and 100 ng mL^{-1} of L1CAM).

silver oxidation, which may contribute to extend the self-life of the Raman probe.

3.2. SERS Response of the Nanoprobes

To monitor the signal enhancement produced by seeding Au-Ag NC or MBA-labelled, AuNCs were tested to monitor L1CAM for C-SPE. The obtained SERS spectra are shown in Figure 3C,D, signaling that the peak at 1078 cm^{-1} was the most adequate to follow the intensity changes in MBA, for concentrations of L1CAM ranging from 0.1 to 100 ng mL^{-1}. The highest L1CAM concentration showed 21 276 and 28 020 Raman intensities when AuNCs (Figure 3C) or AgNCs (Figure 3D) were used, respectively, corresponding to a 31% signal increase; at the lowest L1CAM concentration, the corresponding signals were 832 and 3157 Raman intensities, respectively. As shown by the comparative results of the two metal nanomaterials, the growth of Ag-based nanostructures around AuNPs favored the SERS signal enhancement by ~4×.

3.3. Electrochemical Studies in MIP

In general, MIP synthesis requires complex formation between L1CAM and a suitable functional monomer, which is subsequently polymerized. After removal of L1CAM, the resulting empty cavities are expected to have a shape and stereochemistry complementary to the imprinted protein. These cavities are therefore able to bind L1CAM, which can be followed up by electrochemical detection.[18]

The first step in the construction of the biosensor was to clean the C-SPE (Figure 1-I). This was done with successive CVs under a sulphuric acid solution. The resulting Nyquist plots and cyclic voltammograms are shown in Figure S1 (Supporting Information). They show increasing R_{ct} values and lower current magnitudes and larger peak-to-peak potential differences, respectively, reflecting the oxidation of the carbon substrate at the surface of the electrode. The signals obtained offer higher reproducibility within different C-SPE units than when using the commercially available C-SPE units without a pre-purification step, corresponding to a relative standard deviation of 0.37%. In addition, the sensing units employed in this work maintained equivalent electrochemical and optical responses throughout 1-year, which further validates the reproducibility of the biosensors.

The next step in the construction of the biosensor was to cast TH onto the working electrode (Figure 1-II). TH belongs to the group of phenothiazine dyes with two amino groups and is a molecule with good electron transfer capacity and high solubility in water. TH acts as a cross-linking element between the carbon (on the SPE) and the polyTH MIP to ensure the formation of a stable MIP film: a) TH binds to the carbon electrode via non-covalent functionalization,[33] by establishing van der Walls interactions between the aromatic rings of carbon and TH; b) TH also allows subsequent binding to L1CAM via hydrogen bonding interactions with the chemical functions containing N-H and O-H atoms. The absorption of TH at the C-SPE was confirmed by the increase in conductivity at the electrode surface (**Figure** 4A), as TH and the redox probe are oppositely charged.

The next step was the MIP assembly (Figure 1-III). There are a variety of strategies for the fabrication of MIP[34] of which surface imprinting by electropolymerisation was chosen. Surface imprinting makes it possible to increase the number of imprinted sites, which can increase sensitivity. This requires the incubation of L1CAM on the C-SPE modified with TH, resulting in electrodes with higher R_{ct} values (Figure 4A). Electropolymerization makes it possible to control the size of the polymer film by controlling the electrochemical parameters such as the scan rate, the number of cycles, and the potential window, which proves to be an advantage in terms of reproducibility.[35] The monomer selected for this purpose was TH,[36] which offers two main advantages in terms of MIP construction. First, it contains two amino groups in alpha positions with N-H bonds that allow the formation of hydrogen bonds with multiple functional groups in L1CAM, facilitating complex formation.[37] Second, it yields a conductive polymer, polythionine (PolyTH), which is expected to improve the electrochemical sensitivity. The higher R_{ct} values observed on the electrodes were indeed due to the formation of PolyTH, as the same electrodes incubated in PhB (instead of TH) and treated the same way showed much lower R_{ct} values.

The MIP of polyTH was obtained by CV, where previous information on the conductive/electroactive properties of TH made the electropolymerization process simple, stable, and satisfactorily reproducible.[38] It was originally assumed that the potential sweep would have an upper limit of 0.9 V, as TH would not polymerize at lower potentials,[39] and that the potential of the electrode should be greater than the potential at which oxidation of the NH_2 groups occurred. In an initial exploration of the potential, a well-defined shoulder peak was observed at a maximum potential of 0.9 V with a pair of new reversible peaks ($E_{pc} = -0.2$ V, $E_{pa} = 0.1$) with potentials between −0.3 and 1.2 V at a scan rate of 0.050 V s^{-1} for 15 cycles (Figure S2, Supporting Information). As the number of cycles increased, a gradual increase in peak height and a tendency toward stabilization of peak current on successive scans was observed, confirming the formation of a polymer film of TH on the C-SPE (Figure S2, Supporting Information). Considering that the peak at ≈0.9 V showed irreversible behavior, the potential range of the CV was narrowed down to obtain only the reversible peaks. A CV between −0.4 and +0.4 V was sufficient to cause the formation of polyTH, as evidenced by the purple color on the surface of the electrode and the electrochemical properties of the electrode (Figure S3, Supporting Information). In terms of the number of cycles that regulate the polymer thickness, the current increases with the number of cycles up to 15, after which the current can be slightly reduced.[40] Therefore, a total number of 15 cycles was chosen as the optimum number of cycles for the experiments. As expected, the Nyquist diagrams of the PolyTH before removal of the template show very low R_{ct} values, which is due to the high conductivity of the polymer materials (Figure 4B).

The subsequent stage was template removal (Figure 1-IV), which was performed with oxalic acid. This chemical treatment may have altered the intrinsic conductivity properties of the polymer films, as the overall R_{ct} values increased. Compared to the NIP, the MIP biosensor has intrinsically higher R_{ct} values (Figure 4B), which could be due to the presence of L1CAM proteins within the polymeric network or the fact that the presence of L1CAM hindered the formation of the polymer.

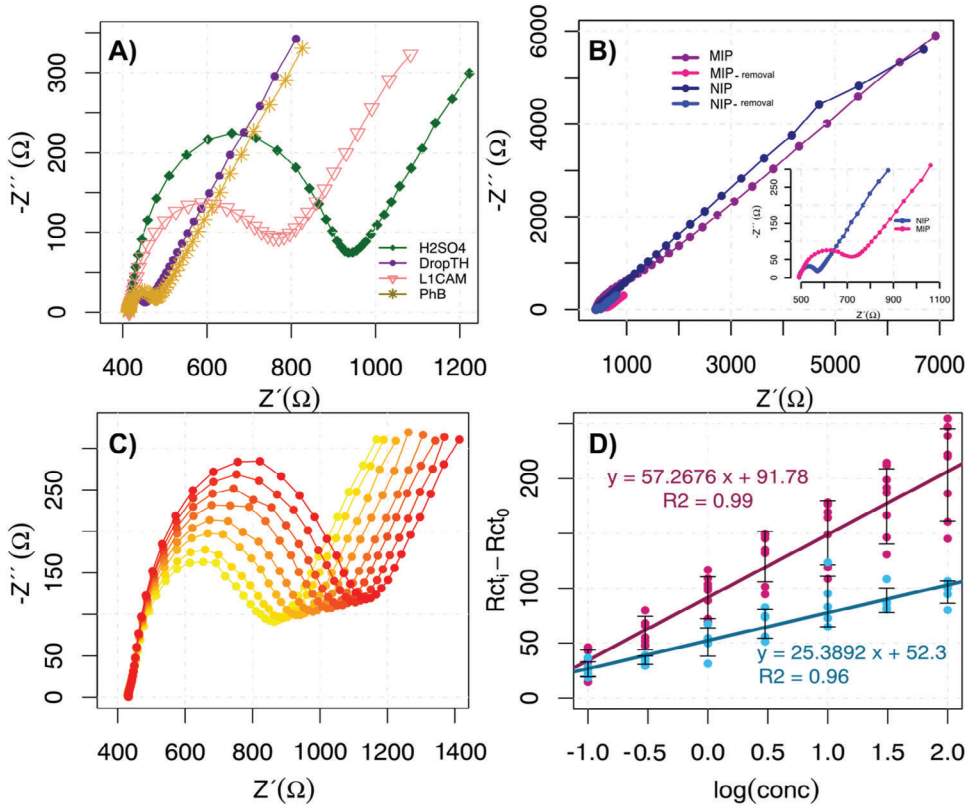

Figure 4. The graphic A) shown the Nyquist plots after cleaning the electrode surface (green), drop casting of TH, 10^{-3} M (violet), and binding of L1CAM, 0.1 mg mL^{-1}, (coral) or PhB pH 7.4 (gold). B) the nyquist plots of the PolyTH films on the electrodes, before and after template removal, and a zoom-in of the data obtained after the L1CAM removal. C) Electrochemical data for calibration with L1CAM standard solutions ranging from 0.1 to 100 ng mL^{-1} prepared in PhB using the MIP biosensor, and the D) corresponding calibration curves with linear plots, for (darkpink) MIP and (lightblue) NIP.

The stability of the signal generated by the sensor was ensured by successive 20-minute incubations in PhB. Only when a stable signal was achieved were the L1CAM standard solutions incubated in the sensor layer to record the calibration curves. The relative standard deviation of the final three readings before proceeding to calibration are typically 0.24%. The concentrations of the L1CAM standard solutions ranged from 0.1 to 100 ng mL^{-1}. As expected, the binding of L1CAM to the complementary MIP cavities contributed to an increase in the R_{ct} value, which was more pronounced with increasing L1CAM concentration (Figure 4C). The greater sensitivity of MIP was confirmed by a slope of ≈57 Ω $decade^{-1}$, compared to less than half the slope of NIP (Figure 4D). This confirms that the dominant response of MIP is due to the binding of L1CAM to the imprinted sites and not to non-specific sites in the polymer film. The linear response of NIP showed much smaller slopes and the quality of the linear fit was poor with a squared correlation coefficient of 0.96.

3.4. SERS Studies in MIP

In the SERS assays, the SERS probe, Au-Ag/MBA/$mSiO_2$/PVP/PDDA/Ab, was incubated in the C-SPE biosensor with a specific concentration of L1CAM. The probe was bound to the electrode surface via the Ab, which binds to the L1CAM already present at the imprinted sites. This binding was evaluated for biosensors with L1CAM concentrations ranging from 0.010 to 31 ng mL^{-1}, tracking the characteristic peak of MBA at 1078 cm^{-1}. For this end, the SERS spectra of each concentration were collected at various locations of the working electrode. The intensity of the SERS signal was also considered to obtain estimated quantitative data on the concentration of L1CAM. Thus, the SERS intensity value at 1078 cm^{-1} (y-axis) was plotted against the logarithm of the L1CAM concentration (x-axis). The use of the logarithmic concentration is related to the typical behavior of MIP materials.

Overall, the spectra exhibited an increasing intensity of the band at 1078 cm-1 with rising protein concentration (**Figure** 5A). This escalation in SERS signal corresponded to a sequence of successive events, commencing with a greater number of probes Au-Ag/MBA/mSiO2/PVP/PDDA/Ab on the surface, binding to a higher quantity of L1CAM protein structures, occupying more binding positions on the MIP. From an analytical standpoint, the results demonstrated an enhancement over the electrochemical technique. While the sensor could detect up to 0.1 ng mL^{-1} L1CAM with the electrochemical technique, SERS detection reached 0.01 ng mL^{-1} (Figure 5B), indicating a tenfold improvement in detection capability.

Since the laser beam only irradiated a small portion of each electrode, it was possible that the SERS signals did not reveal a

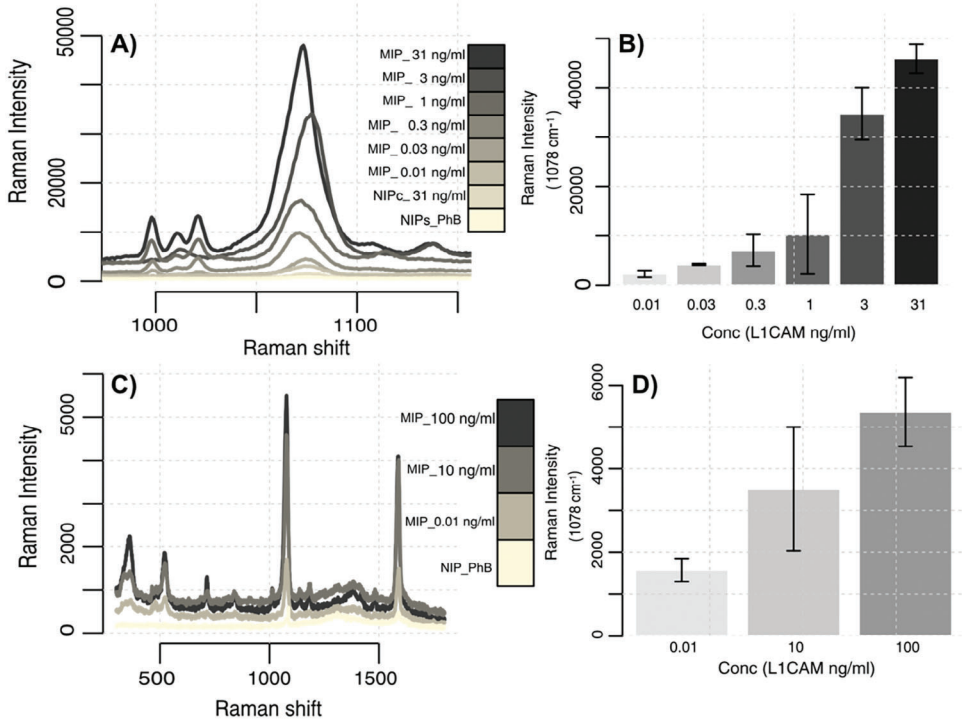

Figure 5. SERS spectra for MIP films incubated with standard solutions of L1CAM of 0.01, 0.03, 0.3, 1, 31 ng mL^{-1} or for NIP films incubated with PhB or 31 ng mL^{-1}. A) Raman spectra ranging from 980 to 1150 cm^{-1}; B) Bar graph for the intensity of the Raman peak at 1078 cm^{-1} for each concentration of L1CAM analyzed in the MIP films. D) SERS spectra obtained using Raman lens to analyze the full electrode area with MIP films incubated with standard solutions of L1CAM of 0.01, 10 and 100 ng mL^{-1} or NIP films incubated with PhB. D) Bar graph for the intensity of the Raman peak at 1078 cm^{-1} for each concentration of L1CAM analyzed in the MIP films.

representative surface of the biosensor. To complement these results, the spectra were also recorded using a macrolens that covered a larger area of the electrode surface. Figure 5D shows the resulting SERS spectra for buffer and L1CAM standard solutions of 0.01, 10, and 100 ng mL^{-1}. In general, it was interesting to note that for buffered solutions incubated at the surface, the Raman signal at 1078 cm^{-1} provided no relevant intensity. As for the response of the MIP to L1CAM, the observed response was also a linear trend as a function of log concentration, suggesting that the surface provided a similar overall response in analytical terms (although the strength of the Raman signal decreased when the signal acquisition conditions were changed).

SEM images were added to the SERS data to understand the differences in the analytical response between MIP and NIP in terms of the density of the nanocapsules on the biosensor surface. The typical images obtained are shown in **Figure 6**. In general, the differences between MIP and NIP electrodes are not obvious when viewed by SEM, but the presence of nanocapsules highlights these differences and signals L1CAM binding sites. The images obtained are in general agreement with the results obtained in SERS. The MIP showed a greater distribution and higher density of AgNCs over the entire surface compared to the NIP. The presence of some AgNCs on the surface of the NIPs indicates non-specific interactions (albeit to a very small extent compared to the MIP). There is also some heterogeneous distribution of the nanocapsules over the electrode surface. This effect is eliminated analytically by having multiple measurement points on each electrode and selecting the most representative response (higher intensity) or a single Raman measurement (lower intensity).

3.5. Serum Study

The biosensor was calibrated in standard solutions prepared in a 100-fold dilution of serum (**Figure 7A**). Foetal bovine serum, which is similar in composition to human serum, was used for this purpose. In general, the serum calibrations showed good analytical properties. They exhibited a linear range from 0.1 to 31 ng mL^{-1}, with a slope of 349 Ω $decade^{-1}$ and a squared correlation coefficient of 0.99 (Figure 7B). The biosensor is sensitive to increasing concentrations of L1CAM, when compared to the analysis made in buffered solutions. This high electrochemical sensitivity was likely due to the presence of additional ionic species in the solutions from the diluted serum and the non-specific binding by coexisting proteins. This was supported by the fact that initial stabilization with a blank solution was very difficult to achieve.

When analyzing the layer that comes into contact with the sample, it was found that the sulfur atom on the TH could undergo side reactions with functional groups in non-specific proteins in the serum. To eliminate this possible non-specific adsorption of components in the serum, a solution of 3-MPA was added to the construction of the MIP prior to protein removal. It was hypothesized that it could bind free -SH in the MIP layer and thus provide a more stable platform against incubation in serum.

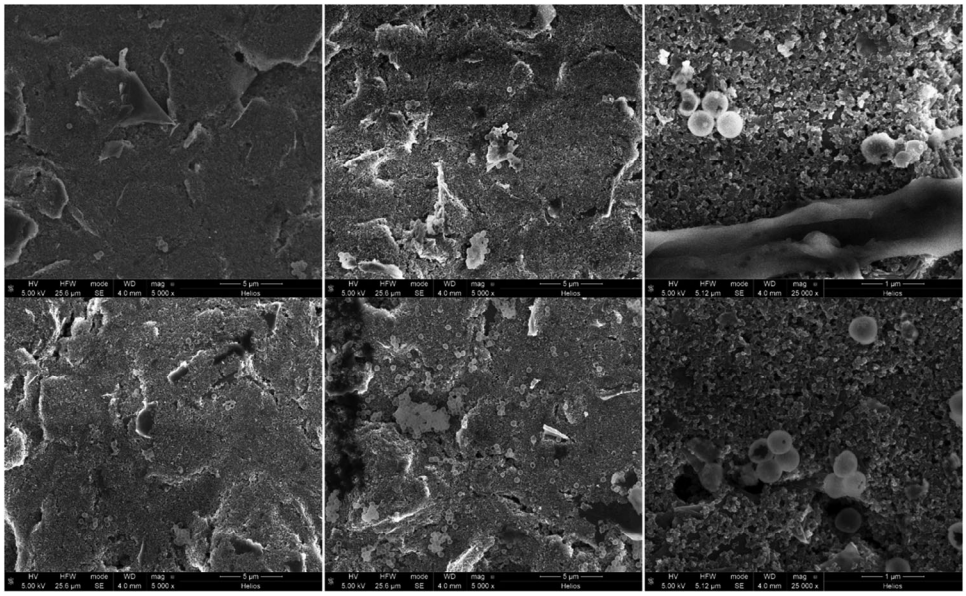

Figure 6. SEM images of the NIP (top, after incubation in buffer solution) and MIP (bottom, after incubation in 100 ng mL^{-1}) films, with Raman probes incubated on the surface of the electrode. The images on the left and in the center correspond to different locations on each electrode; the image on the right corresponds to a higher magnification.

As expected, an improvement in the stabilization of the MIP layer incubated with serum was observed, but this addition of a new layer led to a change in the signal during calibration.

As shown in Figure 7C, with the successive increase in L1CAM concentration two incomplete semicircles became visible. This was reflected in the frequency/phase plots, in Figure 7D,E, where this behavior was much more pronounced for the MIP. Using data for a fixed frequency of 2.95 Hz, the linear curve obtained for the MIP was very different from that of the NIP, corresponding to a linear range from 0.3 to 100 ng mL^{-1} with more than double the sensitivity (Figure 7F). Thus, an increase in the phase value with increasing L1CAM concentration is observed, with the R-squared being 0.99.

3.6. Selectivity Study

Selectivity studies were performed to understand the ability of the analytical system to discriminate between L1CAM and co-existing compounds in biological fluids. The potential interferents selected for this study were creatinine, glucose, and CA 19-9 and their concentrations were adjusted to 1.0×10^{-3} g mL^{-1}, 7.0×10^{-4} g mL^{-1}, and 37 U mL^{-1}, respectively. These solutions were prepared in PhB and incubated separately on the sensor for 20 min. This is the same time given for the standard solutions of L1CAM in the calibration procedure. These results of the separate incubation of the individual interfering substances were compared with the response of the device to L1CAM (10 ng mL^{-1}).

The average percentage of the response was 1.3% for creatinine, 9.9% for glucose, and 10.8% for CA 19-9, compared to L1CAM, indicating a negligible interfering effect (Figure S4, Supporting Information). This was an excellent result considering that this separate interference test corresponds to the worst-case scenario of the device, as the lack of competition with the target molecule could allow a significant non-specific response.

In general, the results obtained showed that MIP has a high selectivity and retains a high affinity for the target molecule in relation to the secondary components.

4. Conclusion

In this study, we have successfully synthesized a novel material featuring a mesoporous silica-based structure encapsulating Au-Ag nanoparticles located at the inner walls of the cavity. This innovative design offers remarkable benefits, including enhanced stability of the Ag particles against oxidation and protection from external contaminants, owing to the presence of the silica shell. By further functionalizing the silver nanoparticles with a Raman tag within the silicon confines, we have achieved precise control over the material's functionality. Notably, the abundance of hot spots within a single nanocapsule has enabled substantial amplification of the SERS signal, underscoring the great potential of this material for sensitive detection applications. These findings pave the way for exciting advancements in the field of nanomaterials and spectroscopic sensing technologies.

In addition to the development of our novel nanomaterial, our study also showcased the construction of a molecularly imprinted polymer (MIP) sensor targeting L1CAM, utilizing polythionine (polyTH) as the sensing element. This MIP sensor exhibited exceptional sensitivity in phosphate buffer (PhB), while pre-treatment with a thiol-based compound was necessary in serum samples to mitigate non-specific binding of coexisting compounds. In terms of advantages of this work compared to other conventional works, it is expected to avoid false results because (i) there is a highly selective binding to the cavity in the MIP (the non-specific absorption in the NIP does not reach

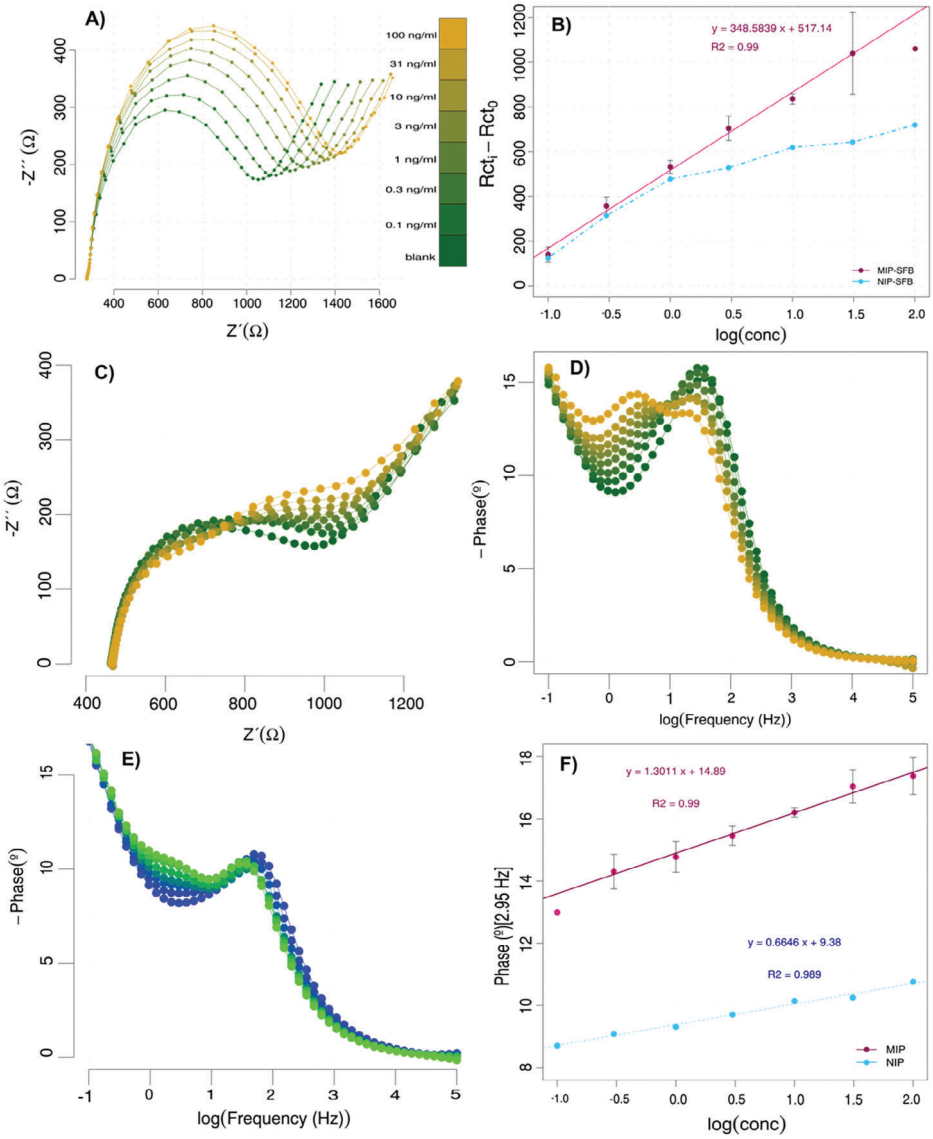

Figure 7. A) Nyquist diagrams for calibration with L1CAM standard solutions ranging from 0.1 to 100 ng mL^{-1} prepared in 100-fold diluted foetal bovine serum using the MIP biosensor. B) Calibration plots for relative R_{ct} to the blank of the MIP (dark pink) and NIP (light blue). C) Nyquist diagrams for calibration with L1CAM standard solutions ranging from 0.1 to 100 ng mL^{-1} prepared in 100-fold diluted foetal bovine serum using the MIP biosensor modified with a layer of 3-MPA. D) Frequency-phase diagram of the MIP. E) Frequency-phase diagram of the NIP. F) Calibration plots for a fixed frequency of 2.95 Hz of the MIP (dark pink) and NIP (light blue).

the values of the corresponding results in the MIP) and (ii) the biorecognition elements employed are of two kinds (plastic antibody and natural antibody, with L1CAM being recognized by each of these). In addition, the production costs are relatively low when compared to works using natural antibodies and there is the possibility of reuse the sensing surface, since the binding in the imprinted cavities is of reversible nature.

Furthermore, our biosensor demonstrated robust electrochemical sensitivity within the clinically relevant range for patients, a response further validated by Raman spectroscopy analysis following the addition of the Raman probe. Leveraging SERS detection, our biosensor exhibited a remarkable 10-fold improvement in detection capacity for the protein. This combined approach of electrochemistry/SERS and MIP/antibodies promises to deliver exceptionally reliable results. The selectivity provided by the MIP is monitored through electrochemical analysis and further confirmed through immunoassay with SERS, enabling a "sandwich-like" assay between a MIP and a naturally derived antibody. This dual detection capability, coupled with dual recognition, holds significant potential for the detection of various biomarkers, particularly in scenarios where minimizing false-positive or false-negative errors is paramount. Thus, the combination of dual detection and recognition capabilities presents promising potential for detecting diverse biomarkers, especially in critical scenarios where reducing false-positive or false-negative errors is crucial.

Supporting Information

Supporting Information is available from the Wiley Online Library or from the author.

Acknowledgements

The authors acknowledge the financial support from the European Commission through the project MindGAP (FET-Open/H2020/GA829040) and YCG (Grant reference SFRH/BD/145590/2019) acknowledges Fundação para a Ciência e a Tecnologia (FCT) for funding. Additionally, this work was funded by Ministerio de Ciencia e Innovación de España (PID2020-113704RB-I00/AEI/10.13039/501100011033; TED2021-132101B-I00/AEI/10.13039/501100011033, PID2020-120306RB-I00/AEI/10.13039/501100011033; PDC2021-121787-I00/AEI/10.13039/501100011033, and Union Europea "NextGenerationEU"/PRTR), HORIZON-EIC-2022-PATHFINDERCHALLENGES-01-06 and HORIZON-HLTH-2022-DISEASE-06-TWO-STAGE, Xunta de Galicia (Centro Singular de Investigación de Galicia – Accreditation 2019–2022 ED431G 2019/06 and IN607A 2018/5), 2020SGR00166 (funded by Generalitat de Cataluña) and 2021PFR-URV-B2-02 (funded by Universitat Rovira I Virgili).

Conflict of Interest

The authors declare no conflict of interest.

Data Availability Statement

The data that support the findings of this study are available from the corresponding author upon reasonable request.

Keywords

biosensor, electrochemistry, molecularly-imprinted polymers, plasmonic nanoparticles, SERS

Received: April 7, 2024
Revised: July 30, 2024
Published online:

[1] Y. C. Cao, Z. Wang, X. Jin, X. F. Hua, M. X. Liu, Y. Di Zhao, *Colloids. Surf. A Physicochem. Eng. Asp.* **2009**, *334*, 53.
[2] J. S. Han, G. S. An, *Nanomaterials.* **2021**, *11*, 3422.
[3] J. Lin, W. Ren, A. Li, C. Yao, T. Chen, X. Ma, X. Wang, A. Wu, *ACS Appl. Mater. Interfaces.* **2020**, *12*, 4204.
[4] S. bin Lee, S. M. Paek, J. M. Oh, *Nanomaterials.* **2021**, *11*, 447.
[5] J. Chen, R. Zhang, L. Han, B. Tu, D. Zhao, *Nano Res.* **2013**, *6*, 871.
[6] Y. Wang, B. Yan, L. Chen, *Chem. Rev.* **2013**, *113*, 1391.
[7] Z. Gao, N. D. Burrows, N. A. Valley, G. C. Schatz, C. J. Murphy, C. L. Haynes, *Analyst.* **2016**, *141*, 5088.
[8] A. Mariño-Lopez, A. Sousa-Castillo, M. Blanco-Formoso, L. N. Furini, L. Rodríguez-Lorenzo, N. Pazos-Perez, L. Guerrini, M. Pérez-Lorenzo, M. A. Correa-Duarte, R. A. Alvarez-Puebla, *ChemNanoMat.* **2019**, *5*, 46.
[9] S. Shim, X. H. Pham, M. G. Cha, Y. S. Lee, D. H. Jeong, B. H. Jun, *RSC Adv.* **2016**, *6*, 48644.
[10] M. Żygieło, P. Piotrowski, M. Witkowski, G. Cichowicz, J. Szczytko, A. Królikowska, *Front. Chem.* **2021**, *9*, 448.
[11] C. Gao, Z. Lu, Y. Liu, Q. Zhang, M. Chi, Q. Cheng, Y. Yin, *Angew. Chem., Int. Ed.* **2012**, *51*, 5629.
[12] M. Zhao, H. Guo, W. Liu, J. Tang, L. Wang, B. Zhang, C. Xue, J. Liu, W. Zhang, *Nanoscale Res. Lett.* **2016**, *11*, 403.
[13] J. E. S. van der Hoeven, H. Gurunarayanan, M. Bransen, D. A. M. de Winter, P. E. de Jongh, A. van Blaaderen, *Adv. Funct. Mater.* **2022**, *32*, 2200148.
[14] D. Lupa, M. Oćwieja, N. Piergies, A. Baliś, C. Paluszkiewicz, Z. Adamczyk, *Colloid Interface Sci. Commun.* **2019**, *33*, 100219.
[15] Z. Pan, J. Yang, W. Song, P. Luo, J. Zou, J. Peng, B. Huang, Z. Luo, *New J. Chem.* **2021**, *45*, 3059.
[16] N. Alizadeh, A. Salimi, *Electroanalysis.* **2018**, *30*, 2803.
[17] M. C. C. G. Carneiro, A. Sousa-Castillo, M. A. Correa-Duarte, M. G. F. Sales, *Biosens. Bioelectron.* **2019**, *146*, 111761.
[18] X. Guo, J. Li, M. Arabi, X. Wang, Y. Wang, L. Chen, *ACS Sens.* **2020**, *5*, 601.
[19] S. Kostrewa, M. Emgenbroich, D. Klockow, G. Wulff, *Macromol. Chem. Phys.* **2003**, *204*, 481.
[20] Y. Lv, Y. Qin, F. Svec, T. Tan, *Biosens. Bioelectron.* **2016**, *80*, 433.
[21] H. Li, X. Wang, Z. Wang, J. Jiang, Y. Qiao, M. Wei, Y. Yan, C. Li, *New J. Chem.* **2017**, *41*, 14342.
[22] Y. Guo, L. Kang, S. Chen, X. Li, *Phys. Chem. Chem. Phys.* **2015**, *17*, 21343.
[23] P. Liu, R. Liu, G. Guan, C. Jiang, S. Wang, Z. Zhang, *Analyst.* **2011**, *136*, 4152.
[24] T. Shahar, T. Sicron, D. Mandler, *Nano Res.* **2017**, *10*, 1056.
[25] X. Tu, P. Muhammad, J. Liu, Y. Ma, S. Wang, D. Yin, Z. Liu, *Anal. Chem.* **2016**, *88*, 12363.
[26] E. González-Domínguez, B. Rodríguez-González, M. Pérez-Lorenzo, M. A. Correa-Duarte, *Nano Res.* **2017**, *10*, 2234.
[27] A. Sousa-Castillo, Ó. Ameneiro-Prieto, M. Comesaña-Hermo, R. Yu, J. M. Vila-Fungueiriño, M. Pérez-Lorenzo, F. Rivadulla, F. J. García de Abajo, M. A. Correa-Duarte, *Nano Energy.* **2017**, *37*, 118.
[28] D. G. Duff, A. Baiker, P. P. Edwards, *J Chem Soc Chem Commun.* **1993**, 96.
[29] M. Sanles-Sobrido, W. Exner, L. Rodrífguez-Lorenzo, B. Rodríguez-González, M. A. Correa-Duarte, R. A. Álvarez-Puebla, L. M. Liz-Marzan, *J. Am. Chem. Soc.* **2009**, *131*, 2699.
[30] Y. Castaño-Guerrero, Y. Romaguera-Barcelay, F. T. C. Moreira, W. R. Brito, E. Fortunato, M. G. F. Sales, *Chemosensors.* **2022**, *10*, 92.
[31] I. Ragheb, M. Braïk, S. Lau-Truong, A. Belkhir, A. Rumyantseva, S. Kostcheev, P. M. Adam, A. Chevillot-Biraud, G. Lévi, J. Aubard, L. Boubekeur-Lecaque, N. Félidj, *Nanomaterials.* **2020**, *10*, 2201.
[32] Z. Gu, S. Tian, Q. Zhou, W. Wei, L. Zhao, X. Li, J. Zheng, *J. Raman Spectrosc.* **2013**, *44*, 1682.
[33] T. A. S. L. de Sousa, T. F. D. Fernandes, M. J. S. Matos, E. N. D. Araujo, M. S. C. Mazzoni, B. R. A. Neves, F. Plentz, *Langmuir.* **2018**, *34*, 6903.
[34] M. Gao, Y. Gao, G. Chen, X. Huang, X. Xu, J. Lv, J. Wang, D. Xu, G. Liu, *Front. Chem.* **2020**, *8*, 1142.
[35] P. Rebelo, E. Costa-Rama, I. Seguro, J. G. Pacheco, H. P. A. Nouws, M. N. D. S. Cordeiro, C. Delerue-Matos, *Biosens. Bioelectron.* **2021**, *172*, 112719.
[36] V. Ferreira, A. Tenreiro, L. M. Abrantes, *Sens. Actuators, B.* **2006**, *119*, 632.
[37] Q. Huang, Z. Zhao, D. Nie, K. Jiang, W. Guo, K. Fan, Z. Zhang, J. Meng, Y. Wu, Z. Han, *Anal. Chem.* **2019**, *91*, 4116.
[38] Z. Jahromi, M. Afzali, A. Mostafavi, R. Nekooie, M. Mohamadi, *Iran. Polym. J.* **2020**, *29*, 241.
[39] Q. Gao, X. Cui, F. Yang, Y. Ma, X. Yang, *Biosens. Bioelectron.* **2003**, *19*, 277.
[40] A. J. S. Ahammad, M. M. Rahman, G. R. Xu, S. Kim, J. J. Lee, *Electrochim. Acta.* **2011**, *56*, 5266.